Theoretical Investigation of Uranyl Dihydroxide: Oxo Ligand Exchange, Water Catalysis, and Vibrational Spectra

Hrant P. Hratchian,*,†,|| Jason L. Sonnenberg,‡,§,⊥ P. Jeffrey Hay,§ Richard L. Martin,§ Bruce E. Bursten,*,‡ and H. Bernhard Schlegel†

Department of Chemistry and Institute of Scientific Computing, Wayne State University, Detroit, Michigan 48202, Department of Chemistry, The Ohio State University, Columbus, Ohio 43210, and Theoretical Division, Los Alamos National Laboratory, Mail Stop B268, Los Alamos, New Mexico 87545

Received: May 18, 2005; In Final Form: July 25, 2005

Density functional theory is employed to investigate uranyl dihydroxide, $UO_2(OH)_2$, isomerization reaction energy barriers, including those occurring via proton shuttles. The ground-state structure of a uranyl dihydroxide complex containing a uranyl moiety with a near 90° O═U═O bond angle is reported for the first time. Furthermore, we predict the vibrational spectra of these compounds. Scalar-relativistic effects for uranium are treated by employing a relativistic effective core potential.

1. Introduction

In the last quarter century of theoretical actinide chemistry, no class of compounds has received more attention than complexes of the uranyl dication, $[UO_2]^{2+}$.[1−3] The formal f^0 nature and abundance of experimental data for this chemistry are primarily responsible for its popularity. One particularly interesting class of uranyl compounds is the set formed by complexation with hydroxide ligands. Uranyl hydroxide chemistry has gained attention in experimental and theoretical communities due to its expected presence in uranium waste solutions. Much of the presented work in this area has focused on uranyl tetrahydroxide, which is the predominant mononuclear species in solutions with a pH greater than 11. Additionally, these compounds are pedagogically interesting because of the strong σ- and π-donor ability of the hydroxide ligand.[4]

Uranyl dihydroxide is a known uranium oxide volatilization product formed in the presence of oxygen and water vapor[5] that might isomerize to form a structure containing an O═U═O bond angle near 90° in the gas phase. Throughout this paper, we refer to structures with a near 90° O═U═O angle as "bent" uranyls; configurations with O═U═O angles near 180° are referred to as "linear" uranyls. Using density functional theory (DFT) calculations, Tsushima and Reich examined two uranyl dihydroxide complexes where both hydroxide hydrogens point toward the same oxo group and the remaining three U coordination sites are occupied by aqua ligands.[6] The *m*-$UO_2(OH)_2(H_2O)_3$ structure, where one aqua ligand is between the two OH^- ligands, was found to be 0.5 kcal mol^{-1} higher in energy than the *o*-$UO_2(OH)_2(H_2O)_3$ structure where the OH^- ligands occupy neighboring coordination sites. Oda and Aoshima confirmed and extended this work by comparing calculated uranyl symmetric stretching frequencies to experimental Raman data.[7] They showed that a dihydroxide configuration with hydrogens pointing toward different oxo groups is slightly favored over the conformation with both hydrogens pointing toward the same oxo ligand.[8] Privalov et al.[9] also reported DFT results reproducing the gaseous $UO_2(OH)_2$ entropy and heat capacity previously determined experimentally by Ebbinghaus using a third law treatment.[10] We also note theoretical work by Clavaguéra-Sarrio et al.[11] that explored a comprehensive series of UO_2X_2 complexes and found OH^- ligands to be the most tightly bound.

In this contribution, we use DFT calculations to investigate the electronic structure of $UO_2(OH)_2$ and to study the energetic accessibility of bent $UO_2(OH)_2$ isomers via oxo ligand exchange reactions, which has been suggested for $UO_2(OH)_4$ in connection with solution chemistries.[12,13] Furthermore, water catalysis for these isomerization processes via proton shuttle reactions is considered, as are the computed vibrational spectra for the key $UO_2(OH)_2$ isomers located on the potential energy surface.

2. Methods

The Gaussian suite of electronic structure programs[14] was used for all calculations. Becke's three-parameter hybrid functional (B3LYP),[15−18] which has been validated in a previous work by Hay and co-workers for uranyl complexes,[19] was employed throughout. To incorporate scalar-relativistic effects, the 60-electron Stuttgart U relativistic effective core potential was employed,[20] while spin−orbit effects have been ignored due to the formal f^0 nature of uranyl complexes. The most diffuse s, p, d, and f Gaussian functions of the associated uranium basis set were removed to generate the [7s 6p 5d 3f] basis, which was used previously.[21−23] The 6-31+G(d,p) basis[24−28] was utilized for the O and H centers. Ground-state and transition structures were optimized using standard methods[29−32] and verified by analytic frequency calculations ensuring that all structures correspond to potential energy surface minima and first-order saddle points, respectively. Using the damped velocity Verlet[33] and Hessian-based predictor−corrector[34,35] integrators of Hratchian and Schlegel, we also confirmed all transition structures reside on a pathway connecting appropriate reactant and product potential energy minima.

* To whom correspondence should be addressed. E-mail: hhratchi@indiana.edu (HPH); bursten@chemistry.ohio-state.edu (BEB).

† Wayne State University.

‡ The Ohio State University.

§ Los Alamos National Laboratory.

|| Present address: Department of Chemistry, Indiana University, Bloomington, IN 47405.

⊥ Present address: Department of Chemistry, Wayne State University, Detroit, MI 48202.

10.1021/jp052616m CCC: $30.25
Published on Web 08/31/2005

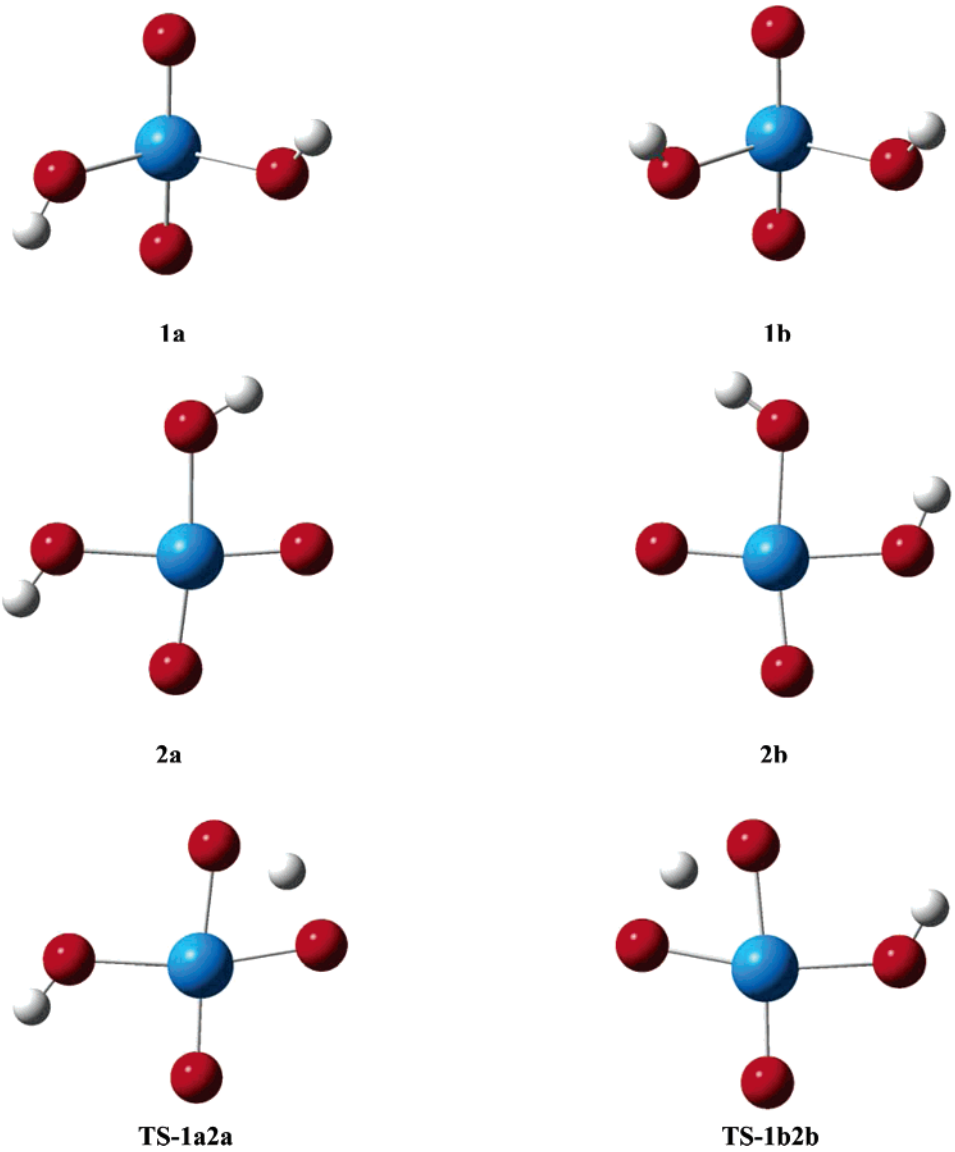

Figure 1. Optimized geometries for **1a**, **1b**, **2a**, **2b**, **TS-1a2a**, and **TS-1b2b**. See Table 1 for geometric parameters.

3. Results and Discussion

The objective of this work is twofold: (1) to understand the nature of structure and bonding in uranyl dihydroxide conformations and (2) to understand the potential for conformational rearrangement. To achieve this, the minimum energy geometries of $UO_2(OH)_2$ are described and the electronic structure of these compounds examined in terms of molecular orbital theory. An intramolecular uranyl dihydroxide isomerization pathway involving oxo ligand exchange is developed along with the potential catalytic role of water in a proton shuttle mechanism of intermolecular isomerization. The vibrational spectra of two key $UO_2(OH)_2$ isomers conclude this section.

Ground-State Geometries and Electronic Structure of $UO_2(OH)_2$. Unconstrained geometry optimizations of linear and bent $UO_2(OH)_2$ structures were carried out from starting geometries in which all seven nuclei were in the same plane. The optimizations yielded the four structures shown in Figure 1. Table 1 gives the energies and geometric parameters for the minimized structures. The calculated gas-phase geometries are in good agreement with related structures previously reported by Tsushima and Reich.[6] Conformers **1a** and **1b**, which have a linear O═U═O linkage and differ only in the orientation of the hydrogen atoms on the hydroxide ligands, are essentially isoenergetic. Conformers **2a** and **2b**, which are bent uranyl complexes, are 16.8 and 18.2 kcal mol^{-1} less stable than **1a**, respectively. As expected, the data in Table 1 clearly indicate that rotation of a U−OH bond (e.g., **1a** ↔ **1b** and **2a** ↔ **2b**) results in negligible alterations of other geometric parameters such as the U═O bond length and O═U═O and HO−U−OH angles.

TABLE 1: Energies and Selected Bond Lengths (Å) and Angles (deg) of 1a, 1b, 2a, and 2b (energies are reported in kcal mol^{-1} relative to 1a)

	1a	1b	2a	2b
energy	0.0	0.0	16.8	18.2
U═O	1.78	1.78	1.82	1.82
U−OH	2.12	2.11	2.09	2.09, 2.10
O−H	0.96	0.96	0.97	0.97
O═U═O	169.4	169.1	99.9	100.0
HO−U−OH	112.3	112.4	86.1	84.1

Perhaps the most notable feature of these structures is the nonlinearity of the HO−U−OH bond angle for **1a** and **1b**, which measures 112°. Additionally, the uranyl subunit is predicted to have a nonlinear angle of 169°. Although these structural features may disagree with intuitive bonding ideas that would otherwise assume a near planar configuration, they are consistent with geometries reported by other authors for

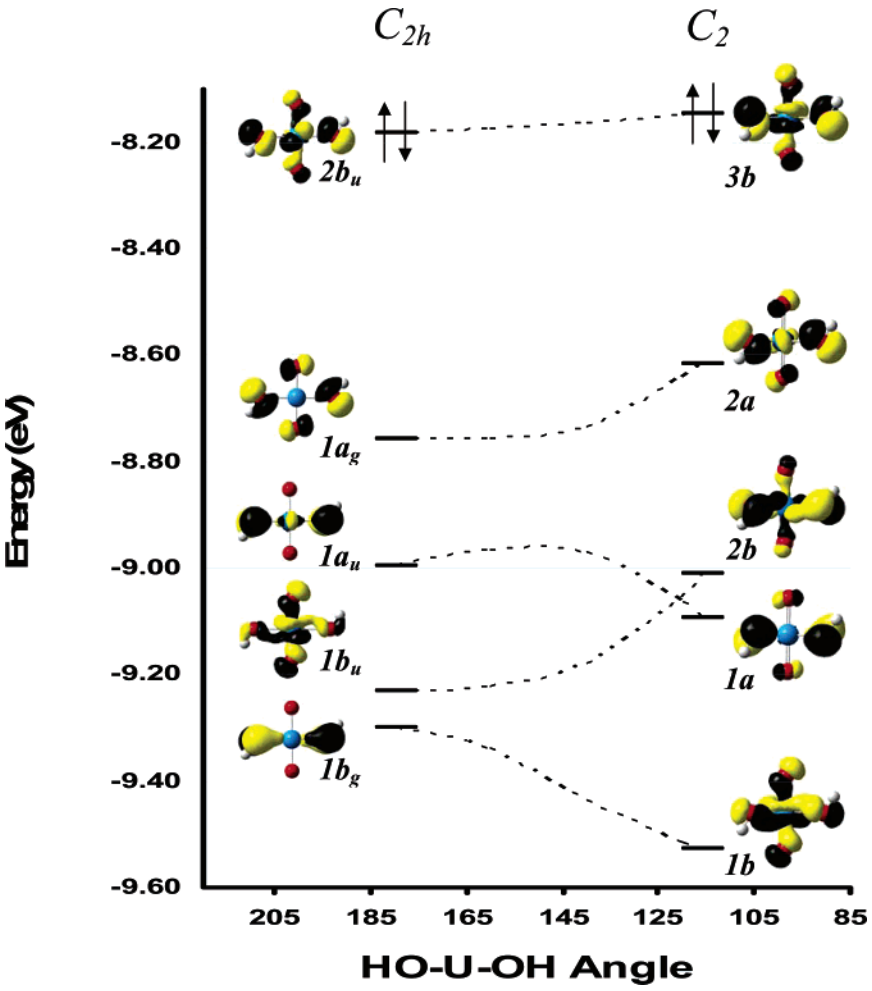

Figure 2. Walsh diagram for **1a** showing orbital energy dependence on HO−U−OH bond angle. For clarity, electron occupation is only shown for the HOMO.

UO_2X_2 compounds. For instance, calculations by Wang and Pitzer[36] have shown that UO_2F_2 has C_{2v} symmetry with a F−U−F angle of 109.7° and an O═U═O angle of 169.5°. In a general bonding study of a large series of UO_2X_2 structures, Marsden and co-workers also showed that compounds in this general class are nonplanar and possess C_2 or C_{2v} symmetry.[11] While these papers have adequately documented the tendency for disubstituted uranyl complexes to display nonlinear X−U−X bond angles, little has been provided by way of molecular orbital theory to explain the trend.

We have constructed a Walsh diagram showing the effect of geometrical perturbation to **1a** along the HO−U−OH internal coordinate (Figure 2). This Walsh diagram shows the energetic changes in the valence molecular orbitals HOMO-4 through HOMO as the HO−U−OH bond angle bends from 180° in an initial planar structure of C_{2h} symmetry to the equilibrium value of 112.3°. As the HO−U−OH bond angle decreases from 180°, the molecular planarity is destroyed, thus lowering the symmetry from C_{2h} to C_2. Adopting the lower symmetry structure decreases the internal energy of the system by 1.92 kcal mol^{-1}. As shown in Figure 2, the energies of the HOMO and HOMO-2 remain nearly constant as the HO−U−OH angle is scanned between 180° and 112.3°. An interesting feature of Figure 2 is the avoided crossing of the C_{2h} $1b_g$ and $1b_u$ as they both transform as b representations when the symmetry is lowered. This avoided crossing yields the 2b and 1b molecular orbitals of the C_2 structure. The result of second-order mixing between the $1b_g$ and $1b_u$ shown for the C_{2h} structure is obvious from inspection of the C_2 orbital representations given in Figure 2. We attribute the C_2 structural preference of $UO_2(OH)_2$ to the stabilization of the 1b orbital, although the very small energy difference between the two geometries does not allow for a definitive explanation based on the Walsh diagram. We believe that a major factor in the stabilization is the small, but significant, U d−f mixing that occurs in the lower symmetry C_2 structure; by contrast, as shown in Tables 2 and 3, there can be no U d−f mixing in the centrosymmetric C_{2h} structure, because the d and f orbitals partition into g and u irreducible representations under C_{2h}. Removal of the inversion center upon lowering the symmetry to C_2 relieves this restriction allowing the d and f orbitals to mix. The data given in Tables 2 and 3 also show that the C_2 molecular orbitals exhibit greater mixing of uranyl and hydroxyl fragment orbitals than those in the C_{2h} structure, again because of the lower symmetry. For example, the HOMO-4 ($1b_g$ and 1b for the C_{2h} and C_2 structures, respectively) has zero character from hydroxide orbitals in the C_{2h} structure, but they make up more than 38% of the molecular orbital character in the C_2 structure. These factors lead to the C_{2v} preference of $UO_2(OH)_2$, and we believe they also account for the generally favored bent X−U−X geometries of other UO_2X_2 compounds.

Both **2a** and **2b** are planar with O═U═O and HO−U−OH angles of ca. 100° and 85°. The bent uranyl unit in these compounds is of particular interest since, to the best of our knowledge, no isolated uranyl compound has displayed this uranyl moiety configuration. Nevertheless, it has been speculated

TABLE 2: Energy (eV) and Mulliken Percent Character for Selected C_{2h} $UO_2(OH)_2$ Molecular Orbitals[a]

		uranium AOs				oxo AOs		O(H) AOs[b]	
MO	energy	s	p	d	f	s	p	s	p
$5a_u$	−1.72		0.8		74.1		1.4		23.4
$2a_g$	−2.47	54.7		39.8		0.2	1.4	−1.9	5.4
$5b_u$	−2.90		−0.4		84.6	1.4	10.8		3.2
$4a_u$	−2.98		0.4		91.3		7.4		0.6
$4b_u$	−3.19		−0.1		97.0	0.6	1.0	0.2	0.2
$3a_u$	−3.28				99.6		0.2		
$3b_u$ (HOMO)	−8.19		4.7		22.2		57.4	−0.4	15.6
$1a_g$	−8.76	−0.2		3.5		1.0	66.4		27.4
$2a_u$	−9.00		1.0		9.3		87.6		1.6
$2b_u$	−9.24		7.8		38.5	0.4	12.0	1.4	38.4
$1b_g$	−9.30			11.7			87.6		
$1a_u$	−10.15	-	1.4		24.2		1.2		73.0
$1b_u$	−10.19		0.8		24.4	1.6	17.4	0.4	54.6

[a] See related Walsh diagram in Figure 2. [b] Contributions from hydrogen basis functions are negligible and not included.

TABLE 3: Energy (eV) and Mulliken Percent Character for Selected C_2 $UO_2(OH)_2$ Molecular Orbitals[a]

	energy	uranium AOs				oxo AOs		O(H) AOs[b]	
MO	(eV)	*s*	*p*	*d*	*f*	*s*	*p*	*s*	*p*
7b	−2.04		−0.1	8.0	69.5	1.4	1.6		19.4
6a	−2.46	18.3	0.8	14.8	43.0	−6.0		9.6	18.6
5a	−3.27	0.2		0.9	90.7	−0.2	5.0	0.8	2.0
6b	−3.29			3.8	89.6		6.0		0.4
5b	−3.43			1.5	97.0		1.0		0.2
4a	−3.44	−0.1		3.0	90.1	1.0	2.2	2.0	1.4
4b (HOMO)	−8.07		3.9	2.5	13.0	0.6	60.8	−0.8	19.2
3a	−8.68	−1.5	0.8	1.7	6.1	0.2	76.8	0.6	14.8
3b	−8.98		1.9	1.0	14.2	0.8	74.6	−0.4	6.8
2a	−9.19		0.3	7.2	2.9	1.0	78.4	-	9.2
2b	−9.55		4.9	3.0	28.4		25.4	1.2	36.4
1a	−10.16	−0.2	1.3	2.9	17.0	0.8	8.8	−0.2	68.8
1b	−10.19		1.5	0.7	23.9	1.6	14.2	0.8	56.4

[a] See related Walsh diagram in Figure 2. [b] Contributions from hydrogen basis functions are negligible and not included.

SCHEME 1

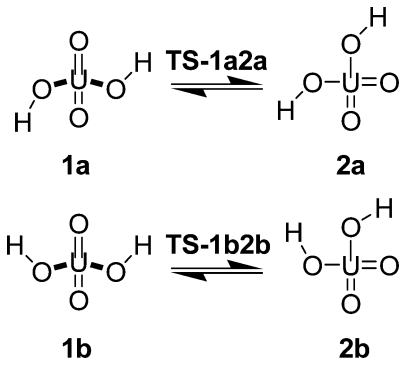

that bent uranyl complexes exist.[12,13] Not only do our calculations indicate that there are minima on the $UO_2(OH)_2$ potential energy surface corresponding to bent uranyl complexes but our results suggest that these compounds, **2a** and **2b**, may be accessible at high temperatures.

Isomerization Reactions. With this structural information in hand, we proceeded to investigate potential modes of intramolecular rearrangement. While a number of multistep processes can be imagined, we focus our attention here on the two elementary, single-step reactions shown in Scheme 1. As discussed below, these processes were initially modeled as gas-phase reactions, that is, without the inclusion (or modeling) of solvent molecules. Conformational conversions aided by explicit water molecules, not contained in the first coordination shell,

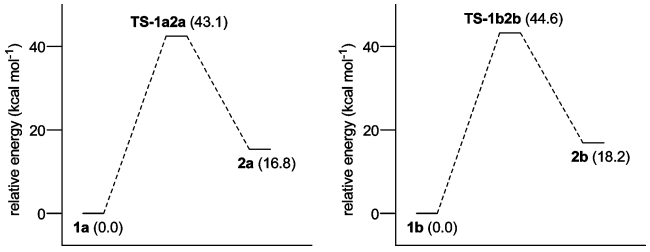

Figure 3. Energy profiles of the **1a** to **2a** and **1b** to **2b** reactions. Values in parentheses are energies relative to **1a** in kcal mol^{-1}.

SCHEME 2

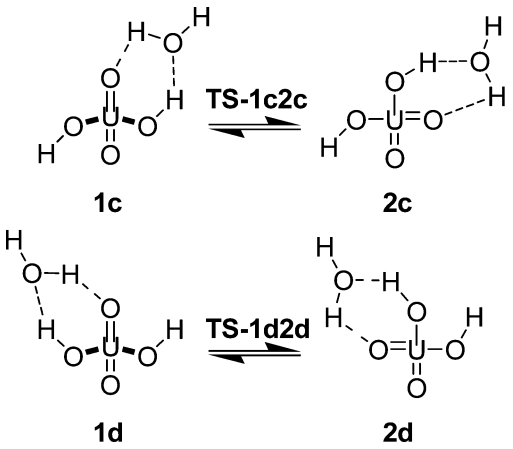

acting as proton shuttles were also considered. It is important to note again that all reported transition structures were fully optimized to verified first-order saddle points on the potential energy surface. We avoided crude approximations to the first-order saddle points based on rigid or relaxed coordinate driving or scan techniques. These approaches are best used to provide useful starting structures for full transition structure optimization. The inadequacy of coordinate driving and scan methods when full optimization is computationally feasible has been discussed in a number of review articles.[29,37−39]

Figure 3 shows the reaction energy profiles for **1a** ⇄ **2a** and **1b** ⇄ **2b**, and Figure 1 gives three-dimensional pictures of the transition structures for these two reactions, **TS-1a2a** and **TS-1b2b**. The transformation of **1a** to **2a** passes through an energy barrier of 43.1 kcal mol^{-1}, whereas the isomerization of **1b** to **2b** has a slightly higher barrier of 44.6 kcal mol^{-1}. While neither reaction would be feasible at room temperature, both isomerization processes may be possible in harsher environments. For instance, it seems reasonable to expect that both reactions occur under the conditions afforded in the incineration of uranium oxide in the presence of oxygen and water vapor where uranyl dihydroxide has been experimentally detected, as mentioned earlier.[5,40−45] We also note that under such conditions, stepwise rearrangements can lead to overall transformations connecting any two of the species considered here since U−OH bond rotations allow for **1a** ⇄ **1b** and **2a** ⇄ **2b**.[46]

On the basis of experimental extended X-ray absorption fine structure data on frozen solutions, Clark et al. proposed that oxo ligand exchange in uranyl hydroxide complexes could be assisted by water molecules acting as proton shuttles.[12] Proton shuttle reactions are known to catalyze a number of organic and biochemical reactions.[47−49] We carried out calculations to ascertain the catalytic effect, if any, of a water molecule serving as a proton shuttle (Scheme 2). As before, full geometry optimizations have been carried out for the $UO_2(OH)_2 + H_2O$

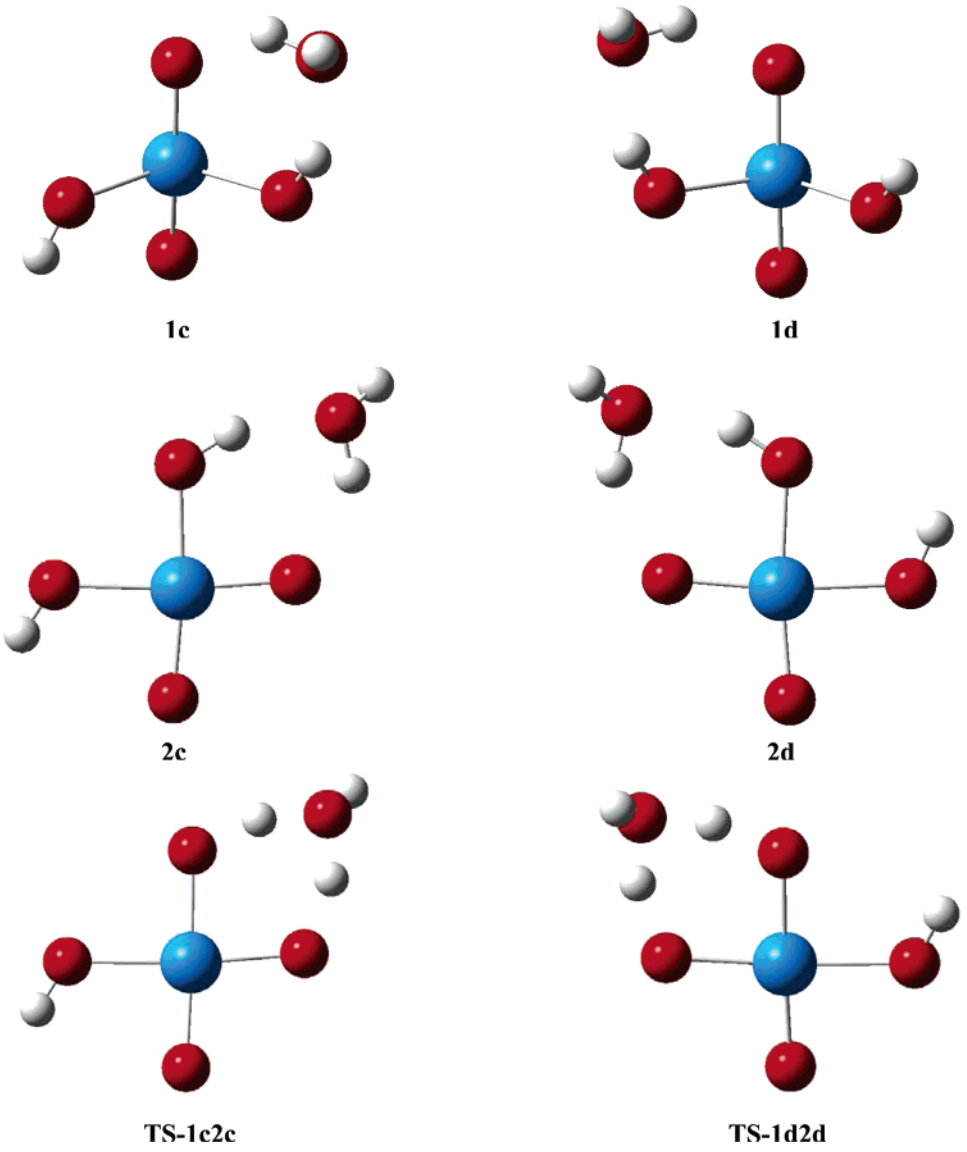

Figure 4. Optimized geometries for **1c**, **1d**, **2c**, **2d**, **TS-1c2c**, and **TS-1d2d**. See Table 4 for geometric parameters.

TABLE 4: Energies and Selected Bond Lengths (Å) and Angles (deg) of 1c, 1d, 2c, and 2d (energies are reported in kcal mol^{-1} relative to 1c)

	1c	1d	2c	2d
energy	0.0	0.3	14.3	15.6
U═O	1.80, 1.79	1.80, 1.78	1.85, 1.82	1.85, 1.81
U−OH	2.09, 2.12	2.09, 2.12	2.04, 2.09	2.06, 2.10
O−H	0.98, 0.97	0.98, 0.97	0.99, 0.97	0.99, 0.97
O═U═O	170.5	169.7	98.8	99.1
HO−U−OH	112.1	113.3	87.1	85.0

adducts and the corresponding proton shuttle transition structures. The adducts of **1a** and **1b** with water have been labeled **1c** and **1d**, respectively. Adducts of **2a**, **2b**, and the isomerization transition structures with water are labeled in like fashion. Minimized geometries of these structures are shown pictorially in Figure 4, key geometric parameters and energies are listed in Table 4, and Figure 5 shows the energy profiles for the reactions in Scheme 2. As shown in Figure 5, the presence of a water molecule acting as a proton shuttle strikingly decreases the reaction barriers for isomerization by roughly 20 kcal mol^{-1}. This result is compatible with the effect of water catalysis via proton shuttle systems in organic and biochemical reactions.[47−66]

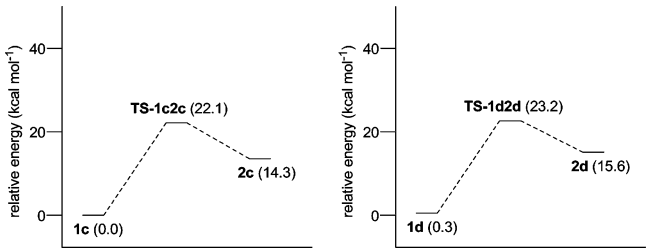

Figure 5. Energy profiles of the **1c** to **2c** and **1d** to **2d** reactions. Values in parentheses are energies relative to **1c** in kcal mol^{-1}.

We note that all attempts to locate transition structures corresponding to isoenergetic dual-ligand-exchange reactions (i.e., **1a** ⇄ **1a**, **2a** ⇄ **2a**, etc.) failed. Similarly, we were unable to find transition structures corresponding to dual-ligand exchange via two water mediated proton shuttles (i.e., **1c** ⇄ **1c**, **2c** ⇄ **2c**, etc.). In every case, our optimizations yielded second- or higher-order saddle points on the potential energy surface. Thus, based on these results, oxo exchange cannot be attributed to concerted motion of the hydroxide hydrogen atoms. Related to these results, previous theoretical work on $UO_2(OH)_4^{2-}$ noted that all attempts to find transition structures for dual-ligand-exchange mechanisms also failed and yielded second-

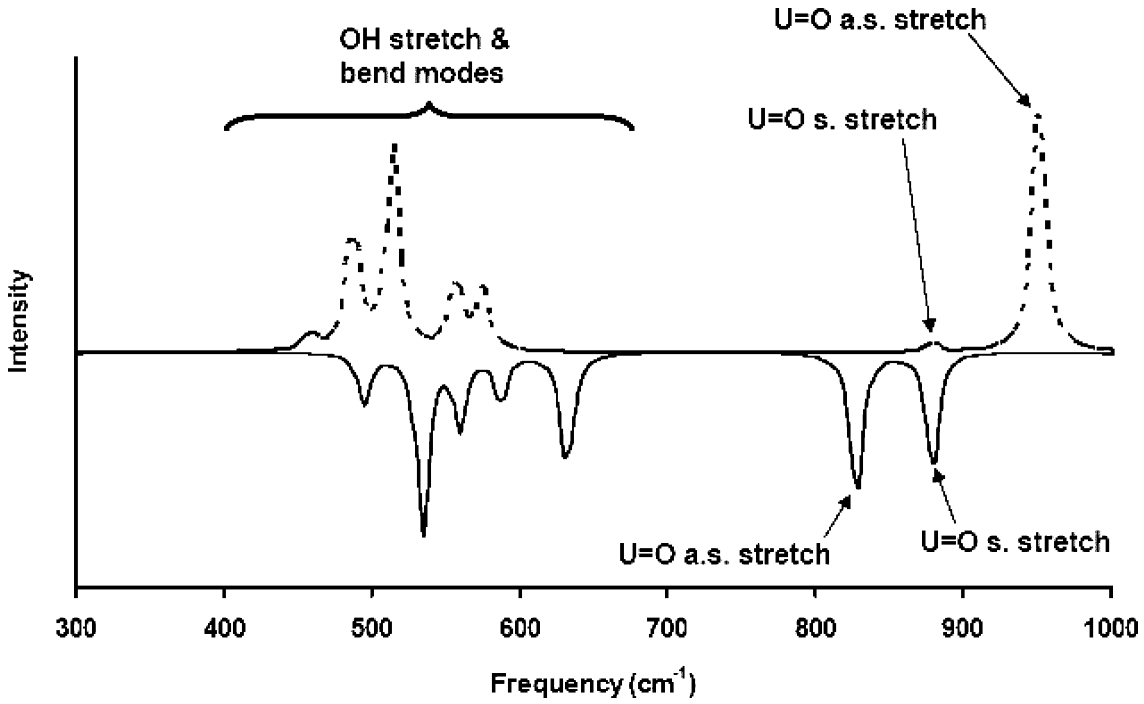

Figure 6. Calculated gas-phase IR spectra of **1a** and **2a**. The top spectrum (dashed line) is **1a** and the bottom spectrum (solid line) is **2a**.

order saddle points.[13] Thus, $UO_2(OH)_2$ ligand exchange reactions proceed preferentially in a sequential manner.

Predicted Vibrational Spectroscopy. From the isomerization studies above, it is clear that the formation of a bent O═U═O angle may be feasible for uranyl dihydroxide under appropriate conditions. Certainly, our results do not provide definitive evidence for an analogous structural motif in other uranyl complexes, but we expect the barriers for isomerization for other uranyl hydroxide complexes to be similar, and preliminary calculations suggest that the isomerization barriers will be further stabilized by solvation. Our results are also consistent with experimental work on $UO_2(OH)_4^{2-}$ and $UO_2(OH)_5^{3-}$ by Clark et al.[12] and theoretical investigations by Schreckenbach, Hay, and Martin.[13]

Infrared (IR) spectroscopy remains one of the principal probes of uranyl complexes, especially in the diagnostic U═O stretching region. The intrinsically different structures of the linear uranyl dihydroxide complexes (**1a** and **1b**) and the bent complexes (**2a** and **2b**) lead naturally to questions about their predicted stretching frequencies. With respect to solution IR spectroscopy, linear uranyl complexes generally show only the strong antisymmetric O═U═O stretch because the symmetric stretch is either formally forbidden or very weak. The bent complexes are expected to exhibit IR-allowed symmetric and antisymmetric stretches that, in the limit of a 90° O═U═O angle, should be roughly equal in intensity. These notions are supported in Figure 6, which shows the calculated gas-phase IR spectra for the linear and bent $UO_2(OH)_2$ structures, **1a** and **2a**. We have also calculated the Raman spectra for **1a** and **2a**, which are shown together in Figure 7. As expected for nearly centrosymmetric compounds, Raman scattering activities are large for modes where the IR intensities are small and vice versa. As a result, the most intense peaks in the Raman spectra for both compounds are bands due to OH symmetric stretching modes (at ∼3850 cm^{-1}, not shown in Figure 7) and bands due to the U═O symmetric stretch modes. Since the U═O symmetric stretch modes appear at the same frequency for **1a** and **2a**, Raman spectroscopy does not discriminate between the linear and bent uranyl structural features as clearly as IR spectroscopy, where the strong peaks due to U═O antisymmetric stretch modes are separated by more than 100 cm^{-1} (see below). Therefore, we focus the remainder of our discussion in this section on IR spectroscopy.

The gas-phase IR spectrum of **1a** can be broken into five vibrational regions. Uranyl bending modes yield bands observed in the far-infrared (not shown in Figures 6 or 7), and U−OH bending modes give rise to a weak peak at 459 cm^{-1} and two stronger intensity peaks at 487 and 514 cm^{-1}; the doublet at 557 and 575 cm^{-1} is due to U−OH stretching modes. A very strong peak is observed at 952 cm^{-1} corresponding to the B antisymmetric uranyl stretch, and the hydroxide stretching modes overlap and give rise to a broad peak centered at ca. 3864 cm^{-1} (not shown in Figures 6 or 7). The A symmetric uranyl stretch in **1a** gives rise to a very weak peak at 879 cm^{-1}; if the molecule had C_{2h} symmetry, then this band would be IR forbidden. Similar assignments exist for the spectrum of **2a**; however, because of the strongly bent O═U═O and HO−U−OH linkages, modes that are (nearly) symmetry forbidden for **1a** are now predicted to be much more intense. In particular, the symmetric A_1 HO−U−OH stretch at 560 cm^{-1} and O═U═O stretch at 879 cm^{-1} are predicted to have significant intensity and no corresponding bands in the linear uranyl complexes. Interestingly, the relative ordering of the symmetric and antisymmetric uranyl stretching bands changes in the **1a** and **2a** vibrational spectra; for **1a**, the antisymmetric stretch is 73 cm^{-1} higher in energy, while the symmetric stretch is 51 cm^{-1} higher in the **2a** spectrum. We also note that the average U═O stretching frequency is 62 cm^{-1} higher in **1a** than in **2a**, which suggests slightly stronger U═O bonding in the linear system.

To understand the origin of the symmetric/antisymmetric uranyl stretch frequency reversal from **1a** to **2a** further, we compared the force constant matrixes of these two compounds. The observed switch in ordering is due to a change in the sign of the U═O/U═O interaction force constant. The difference in

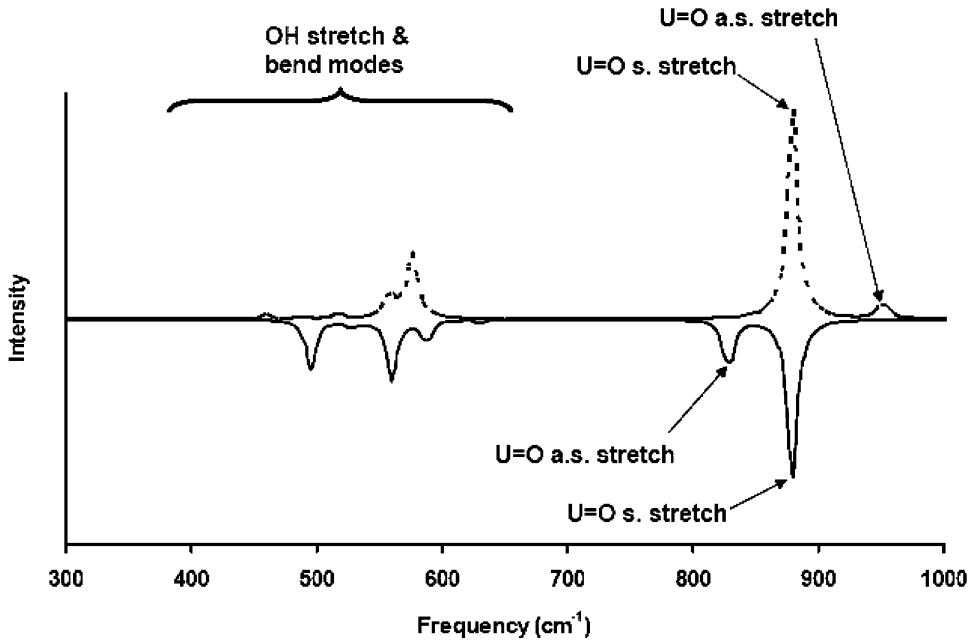

Figure 7. Calculated gas-phase Raman spectra of **1a** and **2a**. The top spectrum (dashed line) is **1a** and the bottom spectrum (solid line) is **2a**.

the splitting of the uranyl symmetric and antisymmetric bands for **1a** and **2a** (73 vs 51 cm^{-1}) is mostly due to differences in the magnitudes of the U═O/U═O interaction force constant, but smaller differences in other off-diagonal terms in the force constant matrix also contribute. The difference between the U═O/U═O interaction force constants in **1a** and **2a** is 0.050 au ($k^{1a}_{U=O,U=O} = -0.010$ au, $k^{2a}_{U=O,U=O} = 0.040$ au). Other key differences between interaction force constants with the U═O coordinates in **1a** and **2a** arise from coupling with the O═U═O bend coordinate ($k^{1a}_{U=O,O=U=O} = 0.010$ au, $k^{2a}_{U=O,O=U=O} = -0.001$ au), the U−OH stretch coordinate ($k^{1a}_{U=O,U-OH} = 0.025$, 0.022 au, $k^{2a}_{U=O,U-OH} = 0.033$, 0.001 au), and the U−O−H bend coordinate ($k^{1a}_{U=O,U-O-H} = 0.006$, −0.002 au, $k^{2a}_{U=O,U-O-H} = 0.010$, −0.005 au). On the basis of Raman spectroscopic data, Nguyen-Trung et al. have reported that a linear correlation can be made between the uranyl stretch frequencies and the average number of equatorial ligands.[7] The nonnegligible U═O/U−OH interaction force constants documented here suggest that this observation may be caused by the coupling between U═O and a varying number of U−OH stretch coordinates. However, charge effects may also be responsible for this trend. It also seems reasonable, based on our results, to expect a similar correlation between the coordination number of a complex containing a bent uranyl subunit. A careful study of these potential effects will be the subject of a future work.

Will it be possible to use these computational results to assist in the unequivocal identification of bent uranyl complexes in solution or in the gas phase? The energy difference between the linear and bent uranyl complexes suggests that an equilibrium between the two will overwhelmingly favor the linear form, and microscopic reversibility requires that the linear-to-bent conversion proceeds in both directions. However, because the bent uranyl complexes are predicted to have strong O═U═O stretching modes in a spectral region that is transparent to the linear complexes, we are hopeful that experimental detection of the bent uranyls by IR spectroscopy might be possible. We hope these results stimulate new experimental investigations of this possibility.

4. Conclusions

In this work, we have used DFT calculations to study the structure, bonding, and relative isomeric stabilities of $UO_2(OH)_2$. Barriers of reaction for isomeric rearrangement processes were also investigated. The results indicate that, consistent with conventional wisdom, isomers containing a linear uranyl subunit are more favored than those containing a bent uranyl arrangement. Free molecule isomerization of uranyl dihydroxide (in the gas phase) from a linear uranyl arrangement to a bent structure seems unlikely under standard conditions. In the presence of water, the results suggest that isomerization and formation of the bent structure may occur via a proton shuttle mechanism. Facilitation of the proton shuttle by a water molecule decreases the barrier of isomerization by roughly 20 kcal mol^{-1} in the gas phase. The current work also includes calculated IR and Raman spectra for $UO_2(OH)_2$ complexes exhibiting linear and bent uranyl moieties. The data clearly indicate that the symmetric O═U═O bond stretch mode can be utilized to detect a bent uranyl unit in $UO_2(OH)_2$, and we have provided detailed spectral information to assist experimentalists in identifying the appropriate vibrational bands.

While the presence of monomeric uranyl dihydroxide is questionable in solution, this system maintains value as a model compound for the more complicated structures that are surely present. The energies of activation computed for isolated $UO_2(OH)_2$ should be similar to those of uranyl hydroxide compounds with higher hydroxide ligand coordination. The vibrational spectra included here should also provide a qualitative description for the vibrational spectra for this family of compounds and may be applicable to the broader $UO_2X_2^m$ structural class.

Acknowledgment. H.P.H. acknowledges the Institute for Scientific Computing at Wayne State University for support provided by a NSF-IGERT fellowship; J.L.S. acknowledges support from the Glenn T. Seaborg Institute at Los Alamos National Laboratory for three Summer Research Fellowships. Los Alamos National Laboratory is operated by the University of California for the U.S. Department of Energy under Contract

W-7405-ENG-36. This work was supported by the National Science Foundation (CHE 0131157 to H.B.S.) and the Division of Chemical Sciences, Geosciences, and Biosciences of the U.S. Department of Energy Office of Basic Energy Sciences (under Grant DE-FG02-01ER15135 to B.E.B. and under the auspices of the Heavy Element Chemistry Program at Los Alamos Laboratory involving P.J.H. and R.L.M.).

Supporting Information Available: Gas-phase energies, unscaled harmonic zero-point vibrational energy corrections, and Cartesian coordinates for each molecule are available. This material is available free of charge via the Internet at http://pubs.acs.org.

References and Notes

(1) Denning, R. G. *Struct. Bonding* **1992**, *79*, 215.
(2) Pepper, M.; Bursten, B. E. *Chem. Rev.* **1991**, *91*, 719.
(3) Schreckenbach, G.; Hay, P. J.; Martin, R. L. *J. Comput. Chem.* **1999**, *20*, 70.
(4) Bursten, B. E.; Casarin, M.; Ellis, D. E.; Fragala, I.; Marks, T. J. *Inorg. Chem.* **1986**, *25*, 1257.
(5) Ebbinghaus, B. B.; Krikorian, O. H.; Fleming, D. L. *Thermodynamic study of $UO_3(g)$, $UO_2(OH)_2(g)$, $UO_2(Cl)_2(g)$, and $UO_2F_2(g)$*; Report No. UCRL-ID-150979; Lawrence Livermore National Laboratory: Livermore, CA, 2002.
(6) Tsushima, S.; Reich, T. *Chem. Phys. Lett.* **2001**, *347*, 127.
(7) Nguyen-Trung, C.; Begun, G. M.; Palmer, D. A. *Inorg. Chem.* **1992**, *31*, 5280.
(8) Oda, Y.; Aoshima, A. *J. Nucl. Sci. Technol.* **2002**, *39*, 647.
(9) Privalov, T.; Schimmelpfennig, B.; Wahlgren, U.; Grenthe, I. *J. Phys. Chem. A* **2002**, *106*, 11277.
(10) Ebbinghaus, B. B. *Calculated thermodynamic functions for gas-phase uranium, neptunium, plutonium, and americium oxides (AnO_3), oxyhydroxides ($AnO_2(OH)_2$), oxychlorides (AnO_2Cl_2), and oxyfluorides (AnO_2F_2)*; Report No. UCRL-ID-122278; Lawrence Livermore National Laboratory: Livermore, CA, 2002.
(11) Clavaguéra-Sarrio, C.; Hoyau, S.; Ismail, N.; Marsden, C. J. *J. Phys. Chem. A* **2003**, *107*, 4515.
(12) Clark, D. L.; Conradson, S. D.; Donohoe, R. J.; Keogh, D. W.; Morris, D. E.; Palmer, P. D.; Rogers, R. D.; Tait, C. D. *Inorg. Chem.* **1999**, *38*, 1456.
(13) Schreckenbach, G.; Hay, P. J.; Martin, R. L. *Inorg. Chem.* **1998**, *37*, 4442.
(14) Frisch, M. J.; Trucks, G. W.; Schlegel, H. B.; Scuseria, G. E.; Robb, M. A.; Cheeseman, J. R.; Montgomery, J. A.; Vreven, T.; Kudin, K. N.; Burant, J. C.; Millam, J. M.; Iyengar, S. S.; Tomasi, J.; Barone, V.; Mennucci, B.; Cossi, M.; Scalmani, G.; Rega, N.; Petersson, G. A.; Nakatsuji, H.; Hada, M.; Ehara, M.; Toyota, K.; Fukuda, R.; Hasegawa, J.; Ishida, M.; Nakajima, T.; Honda, Y.; Kitao, O.; Nakai, H.; Klene, M.; Li, X.; Knox, J. E.; Hratchian, H. P.; Cross, J. B.; Bakken, V.; Adamo, C.; Jaramillo, J.; Gomperts, R.; Stratmann, R. E.; Yazyev, O.; Austin, A. J.; Cammi, R.; Pomelli, C.; Ochterski, J. W.; Ayala, P. Y.; Morokuma, K.; Voth, G. A.; Salvador, P.; Dannenberg, J. J.; Zakrzewski, V. G.; Dapprich, S.; Daniels, A. D.; Strain, M. C.; Farkas, O.; Malick, D. K.; Rabuck, A. D.; Raghavachari, K.; Foresman, J. B.; Ortiz, J. V.; Cui, Q.; Baboul, A. G.; Clifford, S.; Cioslowski, J.; Stefanov, B. B.; Liu, G.; Liashenko, A.; Piskorz, P.; Komaromi, I.; Martin, R. L.; Fox, D. J.; Keith, T.; Al-Laham, M. A.; Peng, C. Y.; Nanayakkara, A.; Challacombe, M.; Gill, P. M. W.; Johnson, B.; Chen, W.; Wong, M. W.; Gonzalez, C.; Pople, J. A. *GAUSSIAN 03*; Gaussian, Inc.: Wallingford, CT, 2003.
(15) Becke, A. D. *Phys. Rev. A* **1988**, *38*, 3098.
(16) Becke, A. D. *J. Chem. Phys.* **1993**, *98*, 5648.
(17) Lee, C. T.; Yang, W. T.; Parr, R. G. *Phys. Rev. B* **1988**, *37*, 785.
(18) Stephens, P. J.; Devlin, F. J.; Chabalowski, C. F.; Frisch, M. J. *J. Phys. Chem.* **1994**, *98*, 11623.
(19) Hay, P. J.; Martin, R. L.; Schreckenbach, G. *J. Phys. Chem. A* **2000**, *104*, 6259.
(20) Küchle, W.; Dolg, M.; Stoll, H.; Preuss, H. *J. Chem. Phys.* **1994**, *100*, 7535.
(21) Han, Y. K.; Hirao, K. *J. Chem. Phys.* **2000**, *113*, 7345.
(22) Hay, P. J. *Faraday Discuss.* **2003**, *124*, 69.
(23) Sonnenberg, J. L.; Hay, P. J.; Martin, R. L.; Bursten, B. E. *Inorg. Chem.* **2005**, *44*, 2255.
(24) Ditchfield, R.; Hehre, W. R.; Pople, J. A. *J. Chem. Phys.* **1971**, *54*, 724.
(25) Gordon, M. S. *Chem. Phys. Lett.* **1980**, *76*, 163.
(26) Hariharan, P. C.; Pople, J. A. *Theor. Chim. Acta* **1973**, *28*, 213.
(27) Hariharan, P. C.; Pople, J. A. *Mol. Phys.* **1974**, *27*, 209.
(28) Hehre, W. J.; Ditchfield, R.; Pople, J. A. *J. Chem. Phys.* **1972**, *56*, 2257.
(29) Hratchian, H. P.; Schlegel, H. B. In *Theory and Applications of Computational Chemistry: The First 40 Years*; Dykstra, C. E., Kim, K. S., Frenking, G., Scuseria, G. E., Eds.; 2005; in press.
(30) Peng, C. Y.; Ayala, P. Y.; Schlegel, H. B.; Frisch, M. J. *J. Comput. Chem.* **1996**, *17*, 49.
(31) Peng, C. Y.; Schlegel, H. B. *Isr. J. Chem.* **1993**, *33*, 449.
(32) Schlegel, H. B. *J. Comput. Chem.* **1982**, *3*, 214.
(33) Hratchian, H. P.; Schlegel, H. B. *J. Phys. Chem. A* **2002**, *106*, 165.
(34) Hratchian, H. P.; Schlegel, H. B. *J. Chem. Phys.* **2004**, *120*, 9918.
(35) Hratchian, H. P.; Schlegel, H. B. *J. Chem. Theory Comput.* **2005**, *1*, 61.
(36) Wang, Q.; Pitzer, R. M. *J. Phys. Chem. A* **2001**, *105*, 8370.
(37) Jensen, F. In *Encyclopedia of Computational Chemistry*; Schleyer, P. v. R., Allinger, N. L., Clark, T., Gasteiger, J., Kollman, P. A., Schaefer, H. F., III, Schreiner, P. R., Eds.; Wiley: Chichester, U.K., 1998; Vol. 5, p 3114.
(38) Jensen, F. *Introduction to Computational Chemistry*; Wiley: Chichester, U.K., 1999.
(39) Wales, D. J. *Energy Landscapes*; Cambridge University Press: Cambridge, U.K., 2003.
(40) Dawson, J. K.; Wait, E.; Alcock, K.; Chilton, D. R. *J. Chem. Soc.* **1956**, 3531.
(41) Francis, A. J.; Dodge, C. J.; Gillow, J. B.; Papenguth, H. W. *Environ. Sci. Technol.* **2000**, *34*, 2311.
(42) Siegel, S.; Hoekstra, H. R.; Gebert, E. *Acta Crystallogr.* **1972**, *B28*, 3469.
(43) Taylor, J. C. *Acta Crystallogr.* **1971**, *B27*, 1088.
(44) Taylor, J. C.; Hurst, H. J. *Acta Crystallogr.* **1971**, *B27*, 2018.
(45) Vier, D. S. A. M. Columbia Report, Report No. A-1277, 1944.
(46) Our test calculations indicate that the barrier to U−OH bond rotation is ca. 5−6 kcal/mol.
(47) Jessop, P. G.; Ikariya, T.; Noyori, R. *Chem. Rev.* **1995**, *95*, 259.
(48) Palmer, D. A.; Vaneldik, R. *Chem. Rev.* **1983**, *83*, 651.
(49) Shaikh, A. A. G.; Sivaram, S. *Chem. Rev.* **1996**, *96*, 951.
(50) Antonczak, S.; Ruizlopez, M. F.; Rivail, J. L. *J. Am. Chem. Soc.* **1994**, *116*, 3912.
(51) Buckingham, A. D.; Handy, N. C.; Rice, J. E.; Somasundram, K.; Dijkgraaf, C. *J. Comput. Chem.* **1986**, *7*, 283.
(52) Lledos, A.; Bertran, J. *Tetrahedron Lett.* **1981**, *22*, 775.
(53) Nguyen, M. T.; Ha, T. K. *J. Am. Chem. Soc.* **1984**, *106*, 599.
(54) Nguyen, M. T.; Hegarty, A. F. *J. Am. Chem. Soc.* **1983**, *105*, 3811.
(55) Nguyen, M. T.; Hegarty, A. F. *J. Am. Chem. Soc.* **1984**, *106*, 1552.
(56) Ventura, O. N.; Lledos, A.; Bonaccorsi, R.; Bertran, J.; Tomasi, J. *Theor. Chim. Acta* **1987**, *72*, 175.
(57) Williams, I. H. *J. Am. Chem. Soc.* **1987**, *109*, 6299.
(58) Williams, I. H.; Spangler, D.; Femec, D. A.; Maggiora, G. M.; Schowen, R. L. *J. Am. Chem. Soc.* **1980**, *102*, 6619.
(59) Williams, I. H.; Spangler, D.; Femec, D. A.; Maggiora, G. M.; Schowen, R. L. *J. Am. Chem. Soc.* **1983**, *105*, 31.
(60) Lewis, M.; Glaser, R. *J. Phys. Chem. A* **2003**, *107*, 6814.
(61) Lewis, M.; Glaser, R. *Chem.−Eur. J.* **2002**, *8*, 1934.
(62) Rodriguez-Santiago, L.; Vendrell, O.; Tejero, I.; Sodupe, M.; Bertran, J. *Chem. Phys. Lett.* **2001**, *334*, 112.
(63) Lin, C. L.; Chu, S. Y. *J. Am. Chem. Soc.* **1999**, *121*, 4222.
(64) Pitarch, J.; Ruiz-Lopez, M. F.; Silla, E.; Pascual-Ahuir, J. L.; Tunon, I. *J. Am. Chem. Soc.* **1998**, *120*, 2146.
(65) Yamabe, S.; Ishikawa, T. *J. Org. Chem.* **1997**, *62*, 7049.
(66) Nguyen, M. T.; Raspoet, G.; Vanquickenborne, L. G.; VanDuijnen, P. T. *J. Phys. Chem. A* **1997**, *101*, 7379.